Original Article

Improved image quality of low-dose CT combining with iterative model reconstruction algorithm for response assessment in patients after treatment of malignant tumor

Xiaoyan Xin[1#], Jingtao Shen[2#], Shangwen Yang[1], Song Liu[1], Anning Hu[1], Bin Zhu[1], Yan Jiang[3], Baoxin Li[1], Bing Zhang[1]

[1]Department of Radiology, [2]Department of Nuclear Medicine, Nanjing Drum Tower Hospital, the Affiliated Hospital of Nanjing University Medical School, Nanjing 210008, China; [3]Clinical Science, Philips Healthcare, Shanghai 200233, China

[#]These authors contributed equally to this work.

Correspondence to: Baoxin Li, MD; Bing Zhang, MD. Department of Radiology, Nanjing Drum Tower Hospital, the Affiliated Hospital of Nanjing University Medical School, Nanjing 210008, China. Email: wangzhi68@163.com; zhangbing_nanjing@vip.163.com.

Background: To evaluate the image quality and radiation dose of low-dose (LD) computed tomography (LD-CT) combining with iterative model reconstruction (IMR) algorithm for response assessment in patients after treatment of malignant tumor compared with routine-dose CT (RD-CT).

Methods: Forty-seven patients [mean age 57.8±10.9 years, 30 males, body mass index (BMI) 22.09±2.35 kg/m^2] after treatment of malignant tumor underwent contrast-enhanced chest and abdomen CT twice for response assessment with an interval of 6 months according to clinical routine. The first CT scans were performed with RD protocol at 120 kVp and images were reconstructed with filtered back projection (FBP) algorithm; while the second scans were performed with LD protocol at 100 kVp and images were reconstructed with FBP and IMR algorithm respectively. All scans were performed using an automatic tube current modulation technique with 150 mAs as reference. Objective image quality including CT attenuation, image noise, and contrast to noise ratio (CNR), and subjective image quality including artifacts, noise, visualization of small structures and confidence of targeted lesions, as well as lesion detection were assessed and compared.

Results: Effective radiation dose of LD-CT scans was reduced 54.8% compared to RD-CT scans (26.89±3.35 *vs.* 12.14±2.09 mSv). Higher CT attenuation was found in both LD-IMR and LD-FBP images compared to RD-FBP images. Better subjective image quality and CNR as well as lower objective noise were found in LD-IMR images (all, $P<0.05$). Two small lesions with the diameter less than 1 cm were missed in LD-FBP images, which were able to be observed in LD-IMR images.

Conclusions: IMR is able to help more than half of reduction of radiation dose without compromising the quality of diagnostic information in patients after treatment of malignant tumors to chest and abdomen CT for response assessment.

Keywords: Radiation dose; low-dose computed tomography (LD-CT); filtered back projection (FBP); model-based; iterative reconstruction (IR)

Submitted Mar 27, 2018. Accepted for publication Aug 10, 2018.
doi: 10.21037/qims.2018.08.05
View this article at: http://dx.doi.org/10.21037/qims.2018.08.05

Introduction

Computed tomography (CT) plays a significant role in tumor diagnosis, staging, and follow-up due to high accuracy, time efficiency, cost considerations, and wide availability of CT scanners (1,2). For patients with malignant tumor, contrast-enhanced chest and abdomen CT scans are widely used in clinical practice for the response assessment, to assess the alleviation, exacerbation, and recurrence of primary lesions as well as the presence of new lesions and/or metastasis (3). However, contrast-enhanced chest and abdomen CT scan are performed with a relatively large scan range and multiple phases, meanwhile, the scans are usually performed more than once to provide useful diagnostic information of tumor progression during the follow-up, which could consequently result in high cumulative doses. Increased ionizing radiation exposure is considered to be related with higher cancer risk (4) and remains a concern in patients with malignancy. Therefore, it is valuable to find an approach that can reduce CT radiation dose while maintaining the image quality and diagnostic accuracy.

Optimization of CT scan parameters including reduced tube voltage and/or tube current and high pitch has been investigated as a useful approach to reduce radiation dose, however, only scan parameters optimization may be also accompanied with deteriorated diagnostic quality of CT images due to their inherent limits of substantial increases of image noise and/or beam-hardening artifacts (5). One solution to improve image quality at low-dose (LD) conditions is the use of advances in reconstruction techniques (6-9), among which the iterative reconstruction (IR) algorithms are widely used. IR algorithms were introduced to help reduce the quantum noise associated with conventional filtered back projection (FBP) algorithms and maintain the image quality. Previous studies demonstrated that images acquired with hybrid-type IR (HIR) algorithms including most of the commercially available IR techniques can maintain image quality with a radiation dose reduction of 23% to 66%, but a certain amount of image noise and artifacts are still present (10,11). In recent years, iterative model reconstruction (IMR, Philips Healthcare), a knowledge-based IR algorithm has been introduced for further dose reduction and image quality improvement, as well as demonstrated significant improvement in low-contrast detectability and artifacts suppression compared to FBP and HIR algorithms at LD scans (12-15).

Hence, we investigated a LD scan protocol with the use of IMR algorithm by comparing the image quality with clinical routine protocol to determine whether the new protocol can result in contrast-enhanced chest and abdomen scans with diagnostic image quality for tumor response assessment.

Methods

The prospective study is approved by Institutional Review Board; informed consent was obtained from all patients.

Study population

We prospectively enrolled 47 consecutive patients who underwent contrast-enhanced chest and abdomen CT twice between August 2015 and March 2016. The inclusion criteria were: (I) diagnosed with malignancy and had received treatment including surgery and/or chemotherapy; (II) being referred for follow-up CT with a maximum interval of 6 months. Exclusion criteria were body mass index (BMI) large than 25 kg/m^2, unstable clinical condition, and life expectancy of less than 6 months.

CT acquisition and image reconstruction

All patients underwent contrast-enhanced chest and abdomen CT twice with an interval of less than 6 months. The first scans were performed on a 64-MDCT scanner (Discovery CT 750HD, GE Healthcare, Milwaukee, USA) with a routine-dose (RD) protocol, while the second scans were performed on a 256-MDCT scanner (Brilliance iCT, Philips Healthcare, Cleveland, Ohio, USA) with a LD protocol. The tube voltage was 120 kV for RD scans and 100 kVp for LD scans, the tube current products were both determined by automatic tube current modulation (ATCM) technique (smart mA from GE Healthcare for RD scans; DoseRight from Philips Healthcare for LD scans), both with 150 mAs as reference. The detector collimation was 64*0.625 for RD scans and 128*0.625 for LD scans. All the other scan parameters were the same in both RD and LD scans: pitch, 0.938; rotation time, 0.75 s; field of view (FOV), 350 mm; slice thickness, 1.0 mm; slice increment, 0.5 mm, matrix 512*512. After non-contrast scans, all patients received intravenous contrast (Ultravist® 370; Schering, Berlin, Germany) at a dose of 1.5 mL/kg and a rate of 4.0 mL/s via a 20-gauge catheter placed in the antecubital vein followed by saline. On the basis of automatic bolus tracking,

tri-phasic scanning commenced 5, 25 and 100 seconds after CT attenuation of the aortic lumen at the level of the celiac trunk, reaching the trigger attenuation threshold of 120 HU. Saline injection was followed by a 30-mL saline flush at the above rate. Images of non-contrast phase, arterial phase (AP), venous phase (VP) and delayed phase (DP) were obtained. The scan range was from apex pulmonis to the lower edge of pubic symphysis during non-contrast phase, from apex pulmonis to the lower pole of kidney during AP, from the top of liver to the lower edge of pubic symphysis during VP, and from the top of liver to the lower pole of kidney during DP, all in a cephalocaudal direction.

Raw data of the first CT scans (RD scans) were reconstructed with FBP algorithm, while those of the second CT scans (LD scans) were reconstructed with FBP and IMR algorithms respectively. There are three levels (L1–L3) provided by IMR algorithms, with L3 providing the maximum noise reduction. In addition, three image modes (Soft-tissue, Routine, SharpPlus) for body parts were provided to fulfill different diagnosis tasks. Here we used the noise level of L1 and image mode of Routine for reconstructions to fulfill the diagnostic task of tumor response assessment, according to our daily practice experience and the previous pilot experiment. At last, three image datasets were ultimately obtained: RD-FBP, LD-FBP, and LD-IMR. All the images were reconstructed with identical parameters of 1.0 mm thickness at 0.5 mm increment. The reconstruction time of 1.0 mm slice thickness IMR images takes approximately 3 to 5 minutes for all scan series per patient.

Image assessment

All images were reviewed and interpreted on a commercially available workstation (Philips Intellispace Portal 6.0). Objective image assessment was performed by a radiologist with 5-year experience on reconstructed 5.0-mm thick axial images of all three image datasets, chest parts were evaluated on images of AP, abdomen parts were evaluated on images of VP. The mean CT attenuation and its standard deviation (SD) of ascending aorta at the level of pulmonary trunk bifurcation, liver parenchyma at the level of portal bifurcation, and anterior abdominal fat were measured via circular regions of interest (ROI). The sizes of ROI in ascending aorta, liver parenchyma were both 100 mm^2, while in anterior, the abdominal fat was 50 mm^2. Image noise of chest ($Noise_c$) was determined as SD of the attenuation of ascending aorta, while of abdomen ($Noise_a$) was determined as the SD of the attenuation of liver parenchyma. Contrast to noise ratio (CNR) of liver parenchyma was calculated using the following formula: $CNR = (\text{mean } HU_{liver} - \text{mean } HU_{fat})/Noise_a$, where mean HU_{liver} and HU fat represented the mean CT value of liver and fat and $Noise_a$ represented the image noise of abdomen.

On the other hand, two experienced radiologists (Xiaoyan Xin with 11 years and Mengru Wang with 4 years of experience) who were not aware of the scan conditions and reconstruction settings, assessed the subjective image quality, independently. Unlike objective image assessment, subjective image assessment was performed on images of all phases and scored overall, according to artifacts, noise, visualization of small structures, and confidence of targeted lesions, using a 5-point scale. The scoring details are as follows: (I) artifacts: 1= severe unacceptable artifacts, 2= major artifacts acceptable under limited conditions, 3= average artifacts not interfering with evaluation of anatomic structure, 4= slightly artifacts, 5= optimal or indicated no artifacts; (II) noise, 1= marked and unacceptable noise; 2= major but acceptable noise, 3= average noise, 4= slightly noise, 5= indicated free noise; (III) visualization of small structures: 1= unacceptable, 2= poor sharpness with blurry edge and structure demarcation, 3= acceptable, the structures demarcation of small vessels and lesions slightly blurry but without impacting of diagnosis, 4= better than average, structure demarcation of small vessels and lesions were displayed clear with sharper edge; 5= excellent, structure demarcation of small vessels and lesions were displayed very clear, sharpest edge; (IV) confidence of targeted lesions: 1= unacceptable, completely non-diagnostic, 2= poor, only suggesting lesion, 3= good, diagnostic, 4= better, diagnostic confidence, 5= excellent, fully diagnostic confidence. When the two radiologists disagreed, a third radiologist with >15 years of experience was asked to adjudicate the differences in order to obtain a consensus score.

Moreover, the number of detected lesions in relevant organs and/or tissues including lung, liver, gallbladder, adrenal glands, pancreas, spleen, kidneys, retroperitoneum, bowel, and bone were recorded. The responses of malignancy after treatment were assessed according to RECIST 1.1 criteria and the results were recorded.

Radiation dose management

Machine-generated CT dose index volume ($CTDI_{vol}$) and scan length were recorded for each patient. The scan length was recorded as scan length chest and scan length abdomen,

Table 1 Comparison of radiation dose between RD-CT and LD-CT scans

Parameters	RD scans	LD scans	P value
Plain scans			
$CTDI_{vol}$ (mGy)	10.65±0.96	4.39±0.34	0.000
Scan length chest (cm)	17.38±1.62	16.27±2.03	0.569
Scan length abdomen (cm)	50.04±4.36	50.48±3.96	0.372
ED (mSv)	10.58±1.28	4.32±0.73	0.000
Arterial phase			
$CTDI_{vol}$ (mGy)	10.65±0.96	4.42±0.47	0.000
Scan length chest (cm)	17.38±1.62	16.27±2.03	0.569
Scan length abdomen (cm)	25.85±2.65	26.73±2.40	0.625
ED (mSv)	4.53±0.67	2.78±0.52	0.000
Portal vein phase			
$CTDI_{vol}$ (mGy)	10.65±0.96	4.51±0.39	0.000
Scan length abdomen (cm)	46.90±3.86	47.35±3.92	0.783
ED (mSv)	7.49±0.86	3.20±0.62	0.000
Delayed phase			
$CTDI_{vol}$ (mGy)	10.65±0.96	4.78±0.52	0.000
Scan length abdomen (cm)	26.85±2.65	25.73±2.40	0.625
ED (mSv)	4.29±0.54	1.84±0.22	0.000
In total			
$CTDI_{vol}$ (mGy)	42.60±3.84	18.10±1.72	0.000
ED (mSv)	26.89±3.35	12.14±2.09	0.000

$CTDI_{vol}$, CT dose index volume; ED, effective radiation dose; RD, routine dose computed tomography; LD, low dose; CT, computed tomography.

with diaphragm as the demarcation. Estimated effective dose (ED) was calculated from $CTDI_{vol}$ multiplied by scan length using a revised normalized ED constant of 0.014 for chest and 0.015 for abdomen (16), respectively:

$ED = CTDI_{vol} \times \text{scan length chest} \times 0.014 + CTDI_{vol} \times \text{scan length abdomen} \times 0.015$.

Statistical analyses

All continuous values are presented as the mean ± SD. To compare the radiation dose between groups, we used student's *t*-test. The objective image quality parameters were compared with one-way ANOVA analysis (17), and if there was a significant difference, pairwise comparisons would be performed with the Dunnett's test (18). The subjective scores were compared by using the Friedman test, and if there was a significant difference, pairwise comparisons would be performed with the Steel-Dwass test (19). Inter-observer agreement for subjective image scores was measured using the kappa test. Lesion numbers were compared using χ^2 test between two reconstruction algorithms in LD scans. All statistical analyses were performed with commercially available software (SPSS Version 15.0), $P<0.05$ was considered to indicate a statistically significant difference.

Results

Patient demographics and radiation dose

Forty-seven patients including 30 males and 17 females,

Table 2 Comparison of objective image quality with different reconstruction in RD and LD scans

Parameters	RD-FBP	LD-FBP	LD-IMR	P value
Attenuation (HU)				
Ascending aorta	167.53±18.95	181.95±14.98*	180.89±13.98*	0.006
Liver	109.39±8.32	118.36±15.20*	119.95±15.60*	0.021
Fat tissue	–41.95±4.04	–30.95±4.14*	–31.89±4.30*	0.035
$Noise_c$ (HU)	10.64±2.07	12.51±3.56*	6.22±1.67*#	0.000
$Noise_a$ (HU)	13.33±2.60	16.40±5.14*	7.65±1.65*#	0.000
CNR	11.35±4.13	9.10±4.46*	19.85±5.16*#	0.000

*, significant difference compared with RD-FBP; #, significant difference compared with LD-FBP. $Noise_c$, image noise of chest; $Noise_a$, image noise of abdomen; RD, routine dose; LD, low dose; FBP, filtered back projection; IMR, iterative model reconstruction.

Table 3 Comparison of subjective image assessment with different reconstruction in RD and LD scans

Parameters	RD-FBP	LD-FBP	LD-IMR	P value	Kappa
Artifacts	4 [3–5]	3 [2–5]	4 [3–5]	0.68	0.78
Noise	4 [2–5]	3 [2–4]*	5 [3–5]*#	0.02	0.85
Visualization of small structures	4 [2–5]	2 [2–3]*	5 [3–5]*#	0.03	0.84
Confidence of targeted lesions	4 [3–5]	3 [2–5]	4 [3–5]	0.09	0.81

Data show the subjective score in a format of median [lower quartile, upper quartile]. *, significant difference compared with RD-FBP; #, significant difference compared with LD-FBP. RD, routine dose; LD, low dose; FBP, filtered back projection; IMR, iterative model reconstruction.

with a mean age of 57.8±10.9 years, a mean BMI of 22.09±2.35 kg/m^2, were investigated in our study. All patients received treatments of surgery and chemotherapy, including 10 patients with lung cancer; 8 patients with hepatic carcinoma; 15 patients with gastric cancer; 6 patients with colorectal cancer; 5 patients with breast cancer; 3 patients with cervical cancer. The results of radiation dose are summarized in *Table 1*. The $CTDI_{vol}$ and effective radiation dose in LD scans were reduced by 57.5% and 54.8% respectively, when compared to RD scans. There was no difference in scan length between LD and RD scans.

Objective image assessment

Table 2 summarizes the results of objective image assessment. CT attenuation of ascending aorta, liver parenchyma, and fat were found higher in both LD-FBP and LD-IMR images compared to RD-FBP images, however, no difference of CT attenuation was found in LD-FBP and LD-IMR images. LD-IMR images exhibited the lowest noise while LD-FBP exhibited the highest noise, in both chest and abdomen scans. CNR was significantly higher in LD-IMR images but lower in LD-FBP images, when compared to RD-FBP images.

Subjective image assessment

The results of subjective image evaluation are summarized in *Table 3*. There was no disagreement between the two radiologists (kappa value =0.78–0.81). No difference was found in artifacts among the three datasets. LD-IMR exhibited the highest score while LD-FBP exhibited lowest score, in noise and visualization of small structures. LD-FBP failed to reach diagnostic acceptable scores (≥3) in visualization of small structures. Lowest confidence was found in LD-FBP images, however, there was no difference in confidence between LD-IMR and RD-FBP images. A representative case is shown in *Figures 1-3*.

Lesion detection and tumor response

A variety of lesions were observed in our study which covers the breadth of diagnoses routinely in patients after

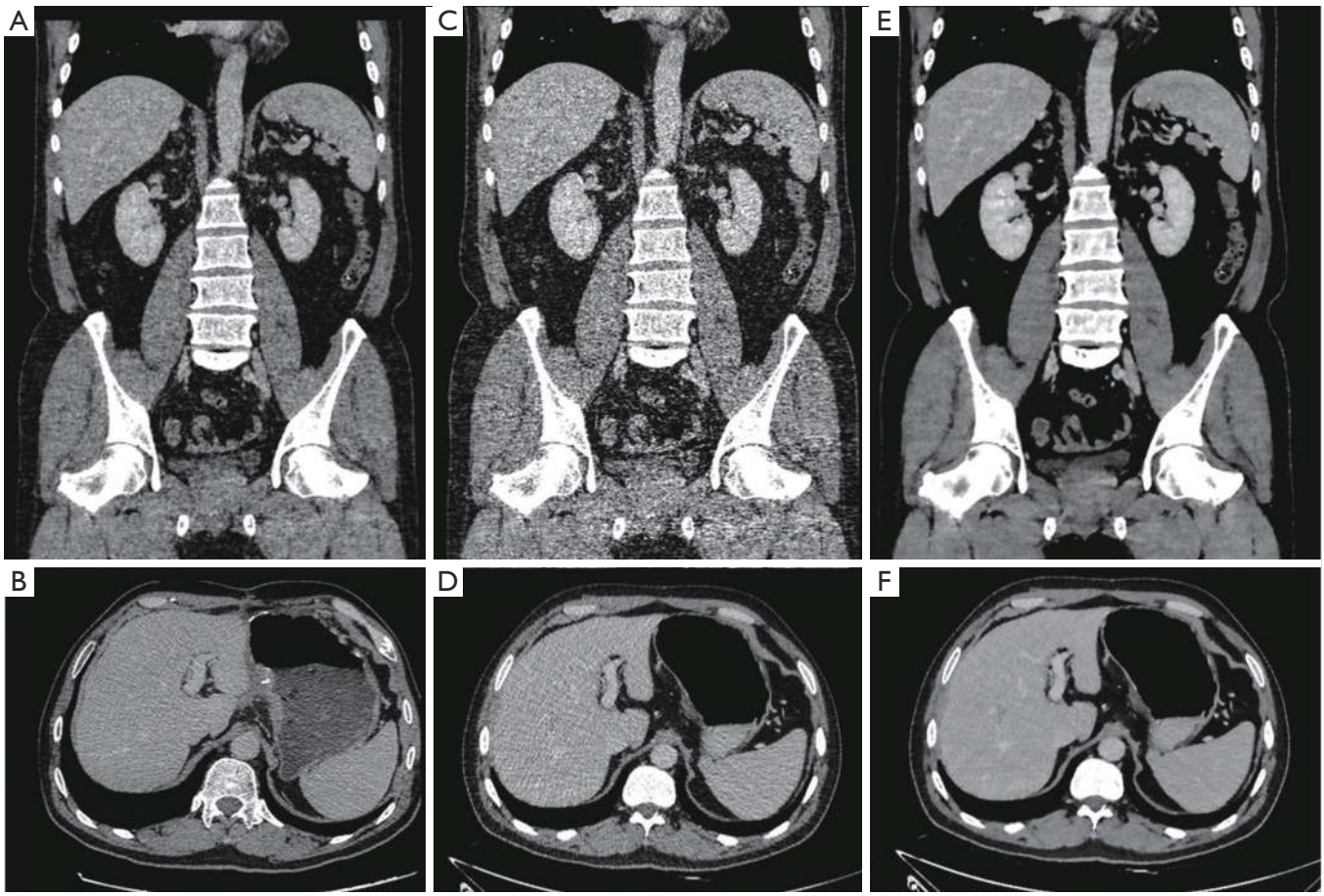

Figure 1 Coronal and axial images of a 52-year-old male after resection and chemotherapy of colon adenocarcinoma (body mass index, 22.5 kg/m^2). The first scans with routine dose and FBP reconstruction (A,B), with the subjective scores of 5, 4, 5, 5 in artifacts, noise, visualization of small structures, and confidence of targeted lesions, respectively. The second scans with low dose and FBP reconstruction (C,D), with significant image noise and fail to reach diagnostic acceptable image quality in visualization of small structures. The second scans with low dose and IMR reconstruction (E,F), with the subjective scores of 5 in all indices. FBP, filtered back projection; IMR, iterative model reconstruction.

treatment of malignancy. The numbers of lesion detected in first and second follow-up scans are summarized in *Table 4*. Results of malignancy response are summarized in *Table 5*. A significant difference was found between LD-FBP and LD-IMR images in numbers of lesion detected in adrenal glands and kidney (P<0.001). One nodule with a diameter of 3 mm in adrenal glands and 1 low attenuation lesion with a diameter of 4 mm in kidney were detected in LD-IMR images however were missed in LD-FBP images, both lesions were observed in their corresponding first scans (RD-FBP). No difference was found in the results of malignancy response that assessed according to LD-IMR and LD-FBP images.

Discussion

In clinical practice, patients with malignancy after treatment often received CT scans 2 to 3 times a year for response assessment, thus could easily have a high burden of radiation dose more than 50mSv with RD scans, which might significantly increase the risk of cancer recurrence or metastasis (20,21). Our study demonstrated an average effective radiation dose of 12 mSv in second follow-up scan with LD protocol, which reduced by more than a half when compared to the first scan with RD protocol, thus being able to minimize the radiation dose to a range of safety.

The LD protocol we adopted is to optimize the scan parameters with reduced tube voltage (100 kV) as well as

Table 4 Lesion detection with different reconstruction in RD and LD scans[a]

Organs	Lesion type	RD-FBP	LD-FBP	LD-IMR	χ^2	P value
Lung	Nodules	26	24	24	N/A	N/A
Liver	Low-attenuation lesions	36	36	36	N/A	N/A
Gall bladder	Wall thickening	8	8	8	N/A	N/A
Adrenal glands	Nodules	12	11	12	6.75	<0.001
Pancreas	Mass	3	3	3	N/A	N/A
Spleen	Low-attenuation lesions	6	6	6	N/A	N/A
Kidney	Low-attenuation lesions	35	34	35	29.29	<0.001
Retroperitoneum	Lymph node	27	26	26	N/A	N/A
Bowel	Wall thickening and obstruction	4	1	1	N/A	N/A
Bone	Mass and destruction	7	6	6	N/A	N/A

[a], numbers represent cases of lesions detection. N/A, not applicable; RD, routine dose; LD, low dose; FBP, filtered back projection; IMR, iterative model reconstruction.

Table 5 Tumor response of all patients according to RECIST 1.1 criteria

Malignant tumor	Response assessment				In total
	CR	PR	SD	PD	
Lung cancer	2	2	4	2	10
Live cancer	0	1	2	5	8
Gastric cancer	2	1	7	5	15
Breast cancer	0	2	2	1	5
Cervical cancer	0	1	1	1	3
Colorectal cancer	1	1	3	1	6
In total	5	8	19	15	47

CR, complete response; PR, Partial response; SD, stable disease; PD, progressive disease.

Figure 2 Axial images of a 51-year-old female after resection and chemotherapy of gastric cancer (body mass index, 20.7 kg/m^2). The first scans with routine dose and FBP reconstruction (A), with the subjective scores of 4, 5, 5, 5 in artifacts, noise, visualization of small structures, and confidence of targeted lesions, respectively. The second scans with low dose and FBP reconstruction (B), with significant image noise and fail to reach diagnostic acceptable image quality in visualization of small structures. The second scans with low dose and IMR reconstruction (C), with the subjective scores of 4, 5, 5, 5. FBP, filtered back projection; IMR, iterative model reconstruction.

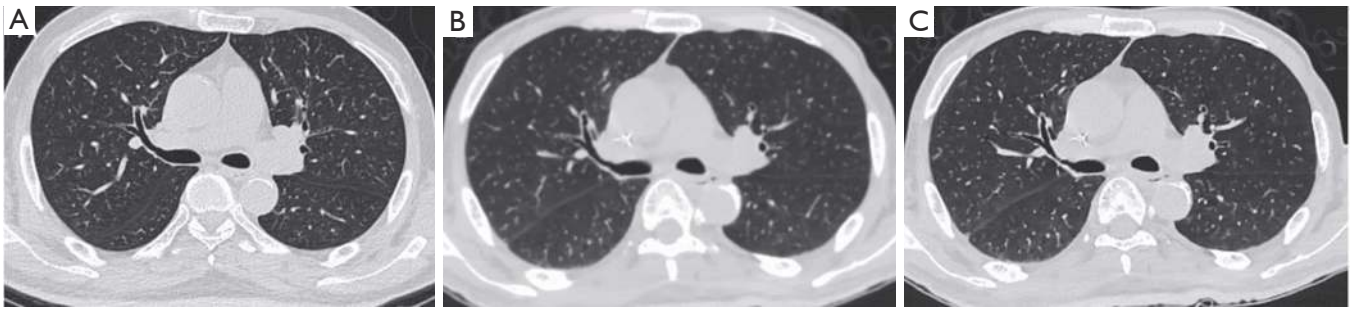

Figure 3 Axial images of a 64-year-old male after resection and chemotherapy of gastric cancer (body mass index, 21.3 kg/m^2). The first scans with routine dose and FBP reconstruction (A), with the subjective scores of 5, 5, 5, 5 in artifacts, noise, visualization of small structures, and confidence of targeted lesions, respectively. The second scans with low dose and FBP reconstruction (B), with the subject scores of 3, 3, 3, 4. Low photon penetration due to low dose was observed as blurred edges and higher noise/artifacts. The second scans with low dose and IMR reconstruction (C), with the subjective scores of all indices. FBP, filtered back projection; IMR, iterative model reconstruction.

ATCM, which can contribute to a significant radiation dose reduction, however theoretically could deteriorate the image quality. Our results revealed that LD images reconstructed with FBP yielded significant image noise and lower CNR and failed to reach diagnostic acceptable image quality in visualization of small structures, which is consistent with theory and previous studies (13,15). However, the LD images reconstructed with IMR yielded lower image noise and better CNR as well as better subjective image quality scores when compared to RD images reconstructed with FBP as reference. IMR is one of the latest generations of commercially available iterative techniques that applies a knowledge-based approach to accurately determine the data and image statistical models that are coupled with the model of the CT system and involve the geometry and physical characteristics of the CT scanner and it may simultaneously provide further radiation dose reduction and improved image quality (12,22). Recent studies have confirmed that IMR images of chest CT acquired at around 1 mSv enables significantly improved image quality compared to FBP and HIR (23), furthermore submSv IMR images in chest scans improve delineation of lesion margins compared to standard-dose FBP (24,25). IMR has also been investigated in LD abdomen CT scans and demonstrated improved image noise and low-contrast resolution (26), moreover, Khawaja *et al.* (15) proposed an ultra-LD protocol in abdomen CT scans with only 0.98 mSv for a single phase and they found that IMR considerably improved both objective and subjective image quality when compared to FBP, but can only be applied in smaller patients and in limited CT indications. In our study, the effective radiation dose of LD scans was around 1mSv for chest parts in a single phase, 3.3 mSv for abdomen parts in a single phase of plain scan and VP, as well as 1.7 mSv for abdomen parts in a single phase of AP and DP. We didn't adopt the ultra-LD protocol since it is of importance to display mediastinal structure and abdominal organs clearly to acquire the tumor-related diagnostic information such as lymph nodes enlargement and new lesions presence, thus the relatively moderate dose reduction protocol was adopted to ensure the diagnostic information acquisition. However, IMR-enabled significant lower image noise, better CNR and better subjective image quality scores in LD-IMR images as compared to RD-FBP images, which was observed in our study and was similar with previous studies, indicates there is still potential to reduce radiation dose further in chest and abdomen CT scans for tumor response assessment.

Both objective and subjective image quality were evaluated in our study. For objective image quality, previous phantom studies (12,27) reported that IMR enabled better spatial resolution and lower curves of noise power spectrum compared to FBP, which was consistent with our results that was IMR enabled lower image noise and higher CNR. For subjective image quality, we evaluated the image noise, artifacts, visualizations of small structures and confidence of targeted lesions, we found that IMR enabled better scores in all indices even in LD-CT scans, meanwhile, we also found that IMR images exhibited a smoother texture, which may be caused by significant noise reduction and the inherent algorithm setting. Additionally, lesion detection between LD-FBP and LD-IMR images were compared. Two small lesions with the diameter less than 1cm were missed in LD-FBP images while were able to be observed in

LD-IMR images, which may be attributed to blurry lesion margins resulted by severe image noise and artifacts in LD-FBP images. It is worth noting that both small lesions can be observed in their corresponding RD-FBP images, which implies LD-IMR images enabling better lesion detection, but not offering high false positive lesion rate. However, the results of malignancy response that assessed according to LD-IMR and LD-FBP images was no difference, the possible reasons could be that the missed lesions are generally small and usually do not affect response results according to RECIST criteria, as well as relatively small sample size.

Our study has several limitations. First, there is an interval of 6 months in each patient between the first RD-CT scans and the second LD-CT scans, causing difficulties to compare lesion features because the malignant lesions after treatment may change at different times, however, there is no difference in baseline characteristics between the two scans, and the image quality assessment can be performed with identical manner, hence, the study results should not be influenced. Second, our study population is relatively small, which may result in some deviations, especially in lesion detection, large sample size may be involved in further studies. Third, we only focused on radiation dose reduction in this study while ignored the optimization of contrast medium amounts, further study may formulate the injection protocol to benefit patients' safety more.

Conclusions

In conclusion, IMR significantly improved the image quality of 50% reduction LD contrast-enhanced chest and abdomen CT scans, which can be used in tumor response assessment, with both diagnostic acceptable image quality and comparable lesion detection ability with routine-dose scans.

Acknowledgements

We thank Dr. Qun Han and Dr. Zhi-Hong Sheng for their technical support in CT scan protocol setting and image quality review.

Funding: This study was partially supported by "Six big talent peak" high-level talent project (No. 2016-WSN-160) from Jiangsu Provincial Department of Human Resources, Jiangsu Province, China, and a research grant of Health Research Projects for Youth (No. Q201411) from Jiangsu Provincial Department of Health, Jiangsu Province, China, and the Social Development Project of Science and Technology in Jiangsu Province (No. BE2016605).

Footnote

Conflicts of Interest: The authors have no conflicts of interest to declare.

Ethical Statement: This prospective study is approved by the Ethics Committee of Nanjing Drum Tower Hospital Affiliated Nanjing University Medical School (No. 2016-065-01); prior informed consent is obtained from all patients.

References

1. De Wever W, Verschakelen J, Coolen J. Role of imaging in diagnosis, staging and follow-up of lung cancer. Curr Opin Pulm Med 2014;20:385-92.
2. Hilton S, Jones LP. Recent advances in imaging cancer of the kidney and urinary tract. Surg Oncol Clin N Am 2014;23:863-910.
3. Wulff AM, Bolte H, Fischer S, Freitag-Wolf S, Soza G, Tietjen C, Biederer J, Heller M, Fabel M. Lung, liver and lymph node metastases in follow-up MSCT: comprehensive volumetric assessment of lesion size changes. Rofo 2012;184:820-8.
4. Zondervan RL, Hahn PF, Sadow CA, Liu B, Lee SI. Body CT scanning in young adults: examination indications, patient outcomes, and risk of radiation-induced cancer. Radiology 2013;267:460-9.
5. Hausleiter J, Meyer T, Hadamitzky M, Huber E, Zankl M, Martinoff S, Kastrati A, Schömig A. Radiation dose estimates from cardiac multislice computed tomography in daily practice: impact of different scanning protocols on effective dose estimates. Circulation 2006;113:1305-10.
6. Liu J, Hu Y, Yang J, Chen Y, Shu H, Luo L, Feng Q, Gui Z, Coatrieux G. 3D Feature Constrained Reconstruction for Low-Dose CT Imaging. IEEE Trans Circuits Syst Video Technol 2018;28:1232-47.
7. Liu J, Ma J, Zhang Y, Chen Y, Yang J, Shu H, Luo L, Coatrieux G, Yang W, Feng Q, Chen W. Discriminative Feature Representation to Improve Projection Data Inconsistency for Low Dose CT Imaging. IEEE Trans Med Imaging 2017;36:2499-509.
8. Chen Y, Shi L, Feng Q, Yang J, Shu H, Luo L, Coatrieux JL, Chen W. Artifact Suppressed Dictionary Learning

for Low-Dose CT Image Processing. IEEE Trans Med Imaging 2014;33:2271-92.
9. Hara AK, Paden RG, Silva AC, Kujak JL,Lawder HJ, Pavlicek W. Iterative reconstruction technique for reducing body radiation dose at CT: feasibility study. AJR Am J Roentgenol 2009;193:764-71.
10. Oda S, Utsunomiya D, Funama Y, Katahira K, Honda K, Tokuyasu S, Vembar M, Yuki H, Noda K, Oshima S, Yamashita Y. A knowledge-based iterative model reconstruction algorithm: can super-low-dose cardiac CT be applicable in clinical settings? Acad Radiol 2014;21:104-10.
11. Nakaura T, Kidoh M, Sakaino N, Utsunomiya D, Oda S, Kawahara T, Harada K, Yamashita Y. Low contrast- and low radiation dose protocol for cardiac CT of thin adults at 256-row CT: usefulness of low tube voltage scans and the hybrid iterative reconstruction algorithm. Int J Cardiovasc Imaging 2013;29:913-23.
12. Mehta D, Thompson R, Morton T, Dhanantwari A, Shefer E. Iterative model reconstruction: simultaneously lowered computed tomography radiation dose and improved image quality. Med Phys Int J 2013;1:147-55.
13. Li T, Zhang Y, Wang Y, Gao J, Jiang Y. Chest CT with iterative reconstruction algorithms for airway stent evaluation in patients with malignant obstructive tracheobronchial diseases. Medicine (Baltimore) 2016;95:e4873.
14. Zhang F, Yang L, Song X, Li YN, Jiang Y, Zhang XH, Ju HY, Wu J, Chang RP. Feasibility study of low tube voltage (80 kVp) coronary CT angiography combined with contrast medium reduction using iterative model reconstruction (IMR) on standard BMI patients. Br J Radiol 2016;89:20150766.
15. Khawaja RDA, Singh S, Blake M, Harisinghani M, Choy G, Karosmangulu A, Padole A, Do S, Brown K, Thompson R, Morton T, Raihani N, Koehler T, Kalra MK. Ultra-low dose abdominal MDCT: using a knowledge-based Iterative Model Reconstruction technique for substantial dose reduction in a prospective clinical study. Eur J Radiol 2015;84:2-10.
16. AAPM REPORT NO. 96 The Measurement, Reporting, and Management of Radiation Dose in CT Report of AAPM Task Group 23: CT Dosimetry Diagnostic Imaging Council CT Committee. Available online: http://www.aapm.org/pubs/reports/RPT_96.pdf
17. Howell DC. Statistical Methods for Psychology (with CD-ROM). 5th edition. Pacific Grove, CA: Duxbury, 2002:324-5. ISBN 0-534-37770-X
18. Dunnett CW. New tables for multiple comparisons with a control, Biometrics 1964;20:482-91.
19. Day RW, Quinn GP. Comparisons of Treatments After an Analysis of Variance in Ecology. Ecol Monogr 1989;59:433-63.
20. Neisius A, Wang AJ, Wang C, Nguyen G, Tsivian M, Kuntz NJ, Astroza GM, Lowry C, Toncheva G, Yoshizumi TT, Preminger GM, Ferrandino MN, Lipkin ME. Radiation exposure in urology: a genitourinary catalogue for diagnostic imaging. J Urol 2013;190:2117-23.
21. Pierce DA, Preston DL. Radiation-related cancer risks at low doses among atomic bomb survivors. Radiat Res 2000;154:178-86.
22. Yuki H, Utsunomiya D, Funama Y, Tokuyasu S, Namimoto T, Hirai T, Itatani R, Katahira K, Oshima S, Yamashita Y. Value of knowledge-based iterative model reconstruction in low-kV 256-slice coronary CT angiography. J Cardiovasc Comput Tomogr 2014;8:115-23.
23. Yuki H, Oda S, Utsunomiya D, Funama Y, Kidoh M, Namimoto T, Katahira K, Honda K, Tokuyasu S, Yamashita Y. Clinical impact of model-based type iterative reconstruction with fast reconstruction time on image quality of low-dose screening chest CT. Acta Radiol 2016;57:295-302.
24. Khawaja RD, Singh S, Gilman M, Sharma A, Do S, Pourjabbar S, Padole A, Lira D, Brown K, Shepard JA, Kalra MK. Computed tomography (CT) of the chest at less than 1 mSv: an ongoing prospective clinical trial of chest CT at submillisievert radiation doses with iterative model image reconstruction and iDose4 technique. J Comput Assist Tomogr 2014;38:613-9.
25. Zhang M, Qi W, Sun Y, Jiang Y, Liu X, Hong N. Screening for lung cancer using sub-millisievert chest CT with iterative reconstruction algorithm: image quality and nodule detectability. Br J Radiol 2017:20170658.
26. Suzuki S, Haruyama T, Morita H, Takahashi Y, Matsumoto R. Initial performance evaluation of iterative model reconstruction in abdominal computed tomography. J Comput Assist Tomogr 2014;38:408-14.
27. Löve A, Olsson ML, Siemund R, Stålhammar F, Björkman-Burtscher IM, Söderberg M. Six iterative reconstruction algorithms in brain CT: a phantom study on image quality at different radiation dose levels. Br J Radiol 2013;86:20130388.

Cite this article as: Xin X, Shen J, Yang S, Liu S, Hu A, Zhu B, Jiang Y, Li B, Zhang B. Improved image quality of low-dose CT combining with iterative model reconstruction algorithm for response assessment in patients after treatment of malignant tumor. Quant Imaging Med Surg 2018;8(7):648-657. doi: 10.21037/qims.2018.08.05

